Vol 18 No 2, February 2009
1674-1056/2009/18(02)/0795-08

Chinese Physics B

© 2009 Chin. Phys. Soc.
and IOP Publishing Ltd

Lateral-field-excitation properties of $LiNbO_3$ single crystal*

Wang Wen-Yan(王文炎)[a], Zhang Chao(张 超)[b]†, Zhang Zhi-Tian(张志甜)[a], Liu Yan(刘 岩)[b], and Feng Guan-Ping(冯冠平)[a,b]

[a] *Department of Precision Instruments and Mechanology, Tsinghua University, Beijing* 100084, *China*
[b] *Center for Information and Optomechatronics, Research Institute of Tsinghua University in Shenzhen, Shenzhen* 518057, *China*

(Received 9 August 2008; revised manuscript received 17 September 2008)

$LiNbO_3$ has been found attractive for lateral field excitation (LFE) applications due to its high piezoelectric coupling. In this paper, bulk acoustic wave propagation properties for $LiNbO_3$ single crystal excited by a lateral electric field have been investigated using the extended Christoffel–Bechmann method. It is found that the LFE piezoelectric coupling factor for c mode reaches its maximum value of 95.46% when $\psi = 0°$ for both (yxl)-58° and (yxwl)±60°/58° $LiNbO_3$. The acoustic wave phase velocity of c mode TSM (thickness shear mode) changes from 3456 m/s to 3983 m/s as a function of ψ. Here ψ represents the angle between the lateral electric field and the crystallographic X-axis in the substrate major surface. A 5 MHz LFE device of (yxl)-58° $LiNbO_3$ with $\psi = 0°$ was designed and tested in air. A major resonance peak was observed with the motional resistance as low as 17 Ω and the Q-factor value up to 10353. The test result is well in agreement with the theoretical analysis, and suggests that the LFE $LiNbO_3$ device can be a good platform for high performance resonator or sensor applications.

Keywords: lateral-field-excitation, $LiNbO_3$, piezoelectric coupling factor, acoustic wave phase velocity

PACC: 7760, 4335

1. Introduction

Bulk acoustic wave devices based on thickness field excitation (TFE) have been widely used in many applications, such as oscillators, filters and sensors for film deposition controls, gas sensing and biochemical liquid measurement, etc.[1−3] TFE devices usually have electrodes on both surfaces of the piezoelectric substrate and employ electric field along the thickness direction to excite thickness shear wave. Figure 1(a) shows a typical structure of a TFE device.

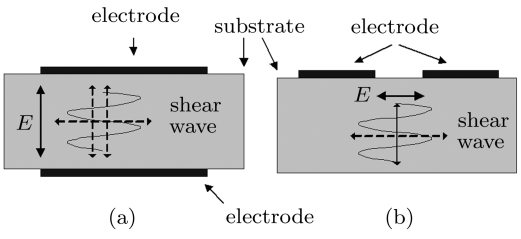


Fig.1. Field excitation mode: (a) TFE and (b) LFE mode.

A lateral field excitation (LFE) device usually has both electrodes on the same surface of the substrate and employs lateral electric field to excite acoustic shear wave, as shown in Fig.1(b). Moreover, LFE devices have also been found attractive in applications for a number of advantages.[4] In particular, there is no electrode in the region of maximum displacement, which results in higher Q values, better frequency stability, and reduced aging of the device. By a judicious placement of the electrodes that results in a particular orientation of the exciting electric field, undesirable modes of certain orientations of the crystal could be totally eliminated. Additionally, certain modes unavailable in the TFE could be excited in the LFE.

Previous research on LFE devices mostly focused on the quartz crystal. Since LFE was first used by Atanasoff and Hart[5] to determine the elastic constants of quartz in the 1940s, the LFE quartz devices have been well investigated and used for high precision frequency control elements, such as resonators.[6] However, the LFE coupling factors in all different cut

*Project supported by the National Natural Science Foundation of China (Grant No 60571014).
†Corresponding author. E-mail: zhangc@tsinghua-sz.edu.cn

orientations for quartz are less than 12%.[4] Its relative permittivity ($\varepsilon_{11} = 4.5$) is also low compared to other common single crystal materials.[7] The two parameters result in a high motional resistance for the LFE quartz device with a typical value as high as 6 kΩ.[8] The high motional resistance has limited its applications in the devices requiring high Q-factor values.

Lithium niobate ($LiNbO_3$) is an extremely versatile nonlinear crystal material, whose electro-optic and nonlinear optical effects have been used for various photonic applications.[9,10] Lithium niobate has also been widely used for surface acoustic wave devices.[11,12] Ballato *et al*[13] have investigated the LFE coupling of lithium niobate and other crystals of 3 m symmetries and found that high LFE coupling factors can be achieved in some special cut orientations of these crystal materials. However, the LFE coupling factor for all different cut orientations was not presented and no experimental result was given for verifying the LFE properties.

In the present paper, wave propagation properties of c mode LFE shear wave have been investigated for all cut orientations and lateral field directions of $LiNbO_3$. LFE devices on (yxl)-58° $LiNbO_3$ have been designed, fabricated and tested. An equivalent circuit model has been used to describe the device's behaviour.

2. Theory

2.1. Piezoelectric coupling factor

For a bulk acoustic wave device, the cut orientation of its substrate is determined by the desired particle polarization mode and its coupling strength expressed by the piezoelectric coupling factor. The coupling factor is important for a piezoelectric device to convert electrical energy to mechanical energy (or *vice versa*). For anisotropic piezoelectric crystals, the piezoelectric coupling factor varies with the cut orientation and the applied electric field direction. The computation of the LFE coupling factor is more complicated than that of TFE due to the increased degree of freedom where the electrode can be arbitrarily oriented in the substrate plane.

The extended Christoffel–Bechmann (C–B) method is used for calculating the LFE piezoelectric coupling factors in all different cut orientations and lateral field directions.[14] The C–B method assumes that acoustic plane waves are propagating in a specified direction with respect to the crystallographic axis of the material. If such waves are confined as standing waves between the two major surfaces of a thin substrate, the ensuing motion of the particle polarization is referred to as simple thickness plate modes.

The IEEE standard is used to define both the crystal axial set and the notation (YXwlt)$\varphi/\theta/\psi$ shown in Fig.2, specifying the orientation of a substrate aligned with a rotated coordinate set of axes. The substrate thickness is taken along the rotated Y'-axis, which is the direction of plane wave propagation. From Fig.2, the substrate is firstly rotated through the angle φ about the Z-axis, then the angle θ about the X-axis, and finally the angle ψ about the Y-axis which is equivalent to the angle between the applied electric field direction and X-axis.

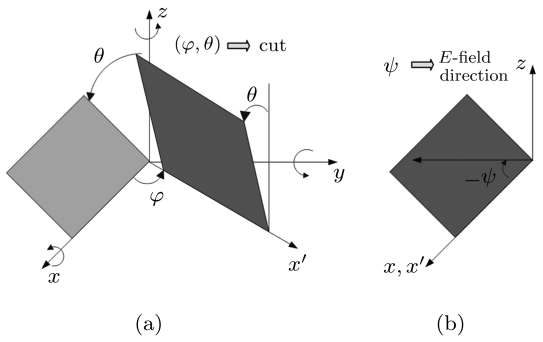


Fig.2. Notation system used for designating (a) crystallographic orientation of a given substrate, and (b) E-field direction relative to the crystallographic axes.

The calculation on $LiNbO_3$ was done using the material constants listed in Table 1. The constitute matrices for a trigonal (3 m) medium which $LiNbO_3$ belongs to are taken in the below calculations. Then using the full tensor forms of the elastic, piezoelectric, and dielectric constants, Γ_{jk}, Ξ_j, Ξ_k, and ε'_{22} are calculated by using Eq.(1), the first equations of Eqs.(2) and (3) respectively for solving the piezoelectrically stiffened elastic constant matrix Γ^*_{jk} for TFE by using Eq.(4).

$$\Gamma_{jk} = c_{ijk\lambda}\alpha_{2i}\alpha_{2\lambda}, \tag{1}$$

$$\Xi_k = e_{ik\lambda}\alpha_{2i}\alpha_{2\lambda}, \quad \Lambda_k = e_{ik\lambda}\alpha_{1i}\alpha_{2\lambda}, \tag{2}$$

$$\varepsilon'_{22} = \varepsilon_{i\lambda}\alpha_{2i}\alpha_{2\lambda}, \quad \varepsilon'_{12} = \varepsilon_{i\lambda}\alpha_{1i}\alpha_{2\lambda},$$

$$\varepsilon'_{11} = \varepsilon_{i\lambda}\alpha_{1i}\alpha_{1\lambda}, \tag{3}$$

$$\Gamma^*_{jk} = \Gamma_{jk} + \Xi_j\Xi_k/\varepsilon'_{22}. \tag{4}$$

Table 1. Material constants for $LiNbO_3$.[7] ε_0 = permittivity of vacuum.

Elastic constants	(10^9 N/m^2)
$c_{11} = c_{22}$	203
$c_{12} = c_{21}$	53
$c_{13} = c_{31} = c_{32} = c_{23}$	75
$c_{14} = c_{41} = -c_{42} = -c_{24}$	9
c_{33}	245
c_{44}	60
Piezoelectric coefficients	(C/m^2)
$e_{15} = e_{24}$	3.7
$e_{22} = -e_{16} = -e_{21}$	2.5
$e_{31} = e_{32}$	0.2
e_{33}	1.3
Relative dielectric constants	
$\varepsilon_{11}/\varepsilon_0 = \varepsilon_{22}/\varepsilon_0$	44
$\varepsilon_{33}/\varepsilon_0$	29
Mass density (ρ)	4700 kg/m^3

In the above equations, $i, j, k, \lambda = 1, 2, 3$; α_{2n} and α_{1n} ($n = i$ or λ) are the elements of the second and first row of the rotation matrix ($\boldsymbol{\alpha}$) respectively; the elastic constant $c_{ijk\lambda}$ and the piezoelectric coefficient $e_{ik\lambda}$ in full subscript form are to be correspondingly replaced with the material constants in Table 1 by using abbreviated subscript notation.[7] By using Γ^*_{jk}, then the eigenvalue equation

$$\left|\Gamma^*_{jk} - c^*\delta_{jk}\right| = 0 \tag{5}$$

is solved, where c^* represents the eigenvector and δ_{jk} is an identity matrix. The roots of the cubic determine the three piezoelectrically stiffened eigenvalues c^*_m, and corresponding eigenvectors $\gamma^{(m)}$, specifying the directions of particle displacement for each mode m, with respect to the crystallographic axes. By tradition, $m = a, b, c$ correspond respectively to the quasi-extensional, the fast- and slow-quasi-shear modes, which are launched by TFE.

However, the effective LFE piezoelectric coupling factor is compounded of both LFE and TFE contributions. For LFE, Λ_n, ε'_{12} and ε'_{11} are calculated by the second equation of Eq.(2) and the last two equations of Eq.(3) respectively. Then, the transformed piezoelectric coefficient and dielectric constant are given by Eqs.(6) and (7) respectively,

$$e'_m = \gamma^{(m)}_n \cdot \left\{\Lambda_n - \left(\frac{\varepsilon'_{12}}{\varepsilon'_{22}}\right) \cdot \Xi_n\right\}, \tag{6}$$

$$\varepsilon''_{11} = \left[\varepsilon'_{11} - \frac{(\varepsilon'_{12})^2}{\varepsilon'_{22}}\right]. \tag{7}$$

Finally, the LFE piezoelectric coupling factors are determined by Eq.(8),

$$k_m(\text{LFE}) = |e'_m| \,/\, \sqrt{\varepsilon''_{11} \cdot c^*_m}. \tag{8}$$

By using Eq.(8), the LFE coupling factors for a, b, and c modes of $LiNbO_3$ in all different cut orientations and lateral field directions, namely as functions of the rotation angles (φ, θ, ψ), can be achieved. The calculated result shows that the maximum LFE coupling factors for a and b modes are 75% and 28% respectively, and are much lower than that for c mode by up to 95.46%. Since the c mode TSM (slow quasi-shear mode) is commonly used in bulk acoustic wave resonators, only its LFE coupling factor K_c is discussed here and its four-dimensional graph is plotted in Fig.3.

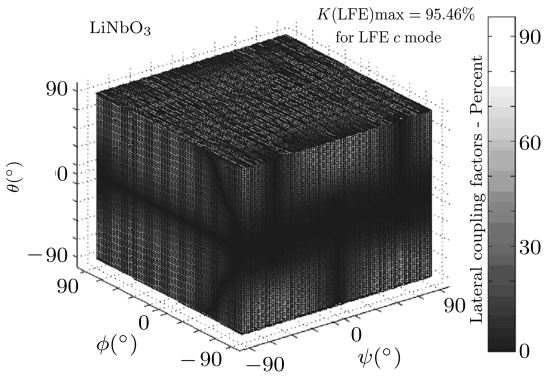


Fig.3. Lateral coupling factor vs. the rotation angles (φ, θ, ψ).

From Fig.3, the K_c value in any cut orientation and lateral field direction of interest can easily be obtained. It has a maximum value of 95.46% when $\psi = 0°$ for the (yxl)-58° or (yxwl)±60°/58° , namely (φ, θ, ψ) = (0°, −58°, 0°) or (φ, θ, ψ) = (±60°, 58°, 0°). The value is far larger than that of the LFE quartz with less than 12%.[4]

Furthermore, the LFE coupling factors for the a, b, and c modes in the (yxl)-58° or (yxwl)±60°/58° $LiNbO_3$ are described in Fig.4. These plots are symmetric about $\psi = 0°$, which reflects an underlying crystallographic symmetry of the (yxl)-58° or (yxwl)±60°/58° $LiNbO_3$ with respect to the X or X' reference axis. It is clear that the LFE coupling factor K_c for c mode reaches its maximum value of 95.46% when $\psi = 0°$ and decreases to 0 when $\psi = \pm 90°$. Both a mode and b mode coupling are very small with their maximum coupling factor value less than 16% and without any coupling at $\psi = 0°$. Therefore, in

order to excite the pure TSM, the electric field angle (ψ) should be equal to 0°, which indicates that the gap generated by the two electrodes should be normal to the crystallographic X-axis.

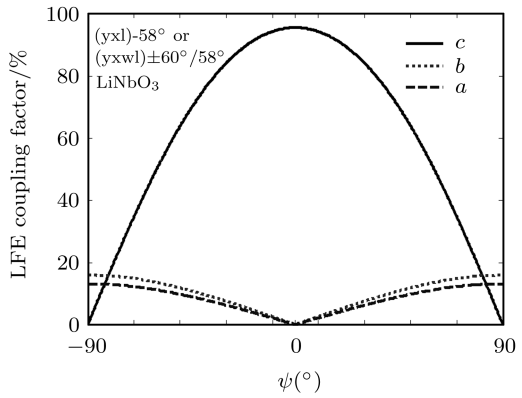


Fig.4. Lateral coupling factor of (yxl)-58° or (yxwl)±60°/58° $LiNbO_3$ as a function of the electric field angle (ψ).

2.2. Acoustic wave phase velocity

According to the piezoelectrically stiffened Christoffel equation,

$$k^2\left(l_{iK}\left\{c^E_{KL}+\frac{[e_{Kj}l_j]\,[l_ie_{iL}]}{l_i\varepsilon^S_{ij}l_j}\right\}l_{Lj}\right)v_j=\rho\omega^2v_i,$$
$$(i,j=1,2,3;K,L=1,2,3,4,5,6), \tag{9}$$

the acoustic wave phase velocity of the TSM launched by the LFE can be derived.[8] Here, k is the wave number; l_{iK} is the wave propagating direction matrix, l_{Lj} is the transpose of l_{iK}, c^E_{KL} is the stiffness constants matrix under the condition of constant electric field, e_{Kj} is the piezoelectric stress constants matrix, e_{iL} is the transpose of e_{Kj}, l_j is the field direction matrix, l_i is the transpose of l_j, ε^S_{ij} is the permittivity constants matrix under the condition of constant strain, v_i is the acoustic wave phase velocity, ρ is the material density; and ω is the angular frequency.

For the (YXwlt)$\varphi/\theta/\psi$ piezoelectric substrate, its acoustic wave phase velocity can be approached in the following way. The method assumes that the acoustic wave propagation is along the rotated Y'-axis and the lateral electric field is impressed along the direction of the angle (ψ) with respect to the rotated X'-axis. Then, the two azimuth cosines in the crystallographic coordinate system, $\boldsymbol{l}_{\rm wave}$ for the wave propagation direction and $\boldsymbol{l}_{\rm E}$ for the electric field direction, are respectively:

$$\boldsymbol{l}_{\rm wave}=\begin{bmatrix}l_{{\rm wave}-x}\\ l_{{\rm wave}-y}\\ l_{{\rm wave}-z}\end{bmatrix}=\begin{bmatrix}-\sin\varphi\cos\theta\\ \cos\varphi\cos\theta\\ \sin\theta\end{bmatrix}, \tag{10}$$

$$\boldsymbol{l}_{\rm E}=\begin{bmatrix}l_x\\ l_y\\ l_z\end{bmatrix}=\begin{bmatrix}\cos\psi\cos\varphi-\sin\psi\sin\theta\sin\varphi\\ \cos\psi\sin\varphi+\sin\psi\sin\theta\cos\varphi\\ -\sin\psi\cos\theta\end{bmatrix}. \tag{11}$$

Then, the matrix l_i is

$$l_i=\boldsymbol{l}_{\rm E} \tag{12}$$

and l_j is the transpose of l_i. The matrix l_{Lj} is determined by $\boldsymbol{l}_{\rm wave}$ and is calculated by using Eq.(13),

$$l_{Lj}=\begin{bmatrix}l_{{\rm wave}-x}&0&0\\ 0&l_{{\rm wave}-y}&0\\ 0&0&l_{{\rm wave}-z}\\ 0&l_{{\rm wave}-z}&l_{{\rm wave}-y}\\ l_{{\rm wave}-z}&0&l_{{\rm wave}-x}\\ l_{{\rm wave}-y}&l_{{\rm wave}-x}&0\end{bmatrix}$$
$$=\begin{bmatrix}-\sin\varphi\cos\theta&0&0\\ 0&\cos\varphi\cos\theta&0\\ 0&0&\sin\theta\\ 0&\sin\theta&\cos\varphi\cos\theta\\ \sin\theta&0&-\sin\varphi\cos\theta\\ \cos\varphi\cos\theta&-\sin\varphi\cos\theta&0\end{bmatrix}, \tag{13}$$

and l_{iK} is the transpose of l_{Lj}. In Eq.(9), the full stiffened Christoffel matrix is

$$\boldsymbol{\Gamma}_{ij}=l_{iK}\left\{c^E_{KL}+\frac{[e_{Kj}l_j]\,[l_ie_{iL}]}{l_i\varepsilon^S_{ij}l_j}\right\}l_{Lj}, \tag{14}$$

where c^E_{KL}, e_{Kj}, ε^S_{ij} are the full tensor forms of the stiffen elastic, piezoelectric strain, and dielectric constants respectively, as listed in Table 1. Then the eigenvalue equation

$$|\boldsymbol{\Gamma}_{ij}-c\delta_{ij}|=0, \tag{15}$$

is solved. And its three eigenvalues c_m are obtained, yielding the acoustic wave phase velocities,

$$v_m=\sqrt{c_m/\rho}, \tag{16}$$

where $m=a,b,c$ correspond respectively to the quasi-extensional, the fast- and slow-quasi-shear modes.

By using Eq.(16), the phase velocity (V_a) for c mode of the (yxl)-58° or (yxwl)±60°/58° $LiNbO_3$ was calculated and plotted in Fig.5. It can be seen that the phase velocity of c mode TSM is a function of the electric field ψ. When $\psi = \pm 90°$, the LFE phase velocity drops to its minimum value of 3456 m/s. When $\psi = 0°$, it reaches its maximum value of 3983 m/s.

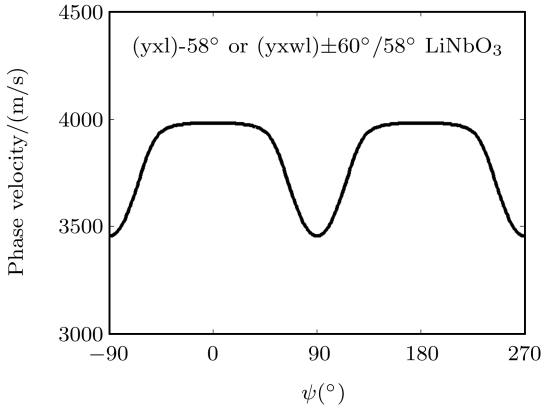


Fig.5. Phase velocity of the TSM excited by the LFE.

device due to its maximum c-mode LFE coupling factor and a pure TSM being able to be excited when $\psi = 0°$. In the study, the LFE device was designed and fabricated, as shown in Fig.6 (left). Its substrate was machined to be 0.455 mm thick, which results in a fundamental frequency of 4376923 Hz for c mode TSM by using Eq.(17).

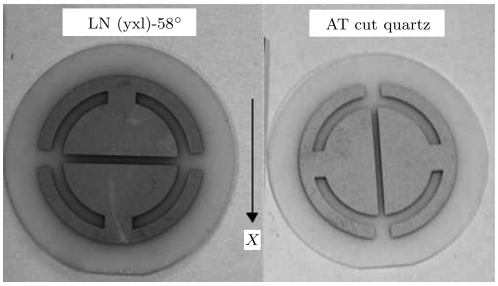


Fig.6. Photos of LFE device: two electrodes in frontal side and bare crystal surface in opposite side. LN stands for $LiNbO_3$.

3. Experimental

In the conventional LFE crystal resonator structure shown in Fig.1(b), electrodes are on one surface of the piezoelectric substrate. Since the electric field is inversely proportional to the gap spacing for a given voltage, the electrode gap plays a very critical role in improving the device performance. As the gap spacing increases, less laterally excited energy is confined to the active region (i.e., the gap region between the two electrodes). If the gap is too small, the spurious mode is easily produced. It has experimentally been observed that the LFE gap spacing should be on the order of the substrate thickness.

For a TSM device, the shear wave propagates back and forth along the thickness direction of the substrate, as shown in Fig.1. If most of the wave are reflected from the top and bottom surfaces of a piezoelectric substrate, a standing wave is formed. An acoustic resonance is obtained at a frequency (f_N),

$$f_N = \frac{N \cdot V_a}{2d}, \tag{17}$$

where N, V_a and d are the positive odd number, the acoustic wave phase velocity and piezoelectric substrate thickness, respectively. When $N = 1$, f_1 is a fundamental resonant frequency.

According to the above calculated results, we choose the (yxl)-58° as the substrate cut for the LFE

The substrate was manufactured by Sichuan Institute of Piezoelectric and Acoustooptic Technology (SIPAT), Chongqing, China. It is a thin disk with a diameter of 25.4 mm. The two electrodes are on one major plane and no electrodes on other side. The electrode was deposited by vacuum evaporation by Shenzhen Kelide Electronic Ltd, Shenzhen, Guangdong Province, China. It consists of about 2 nm thickness adhesion layer of chromium followed by about 200 nm thickness of gold. Each electrode is semi-circled with 12.7 mm in diameter and is separated by a gap of 1 mm. The electrode gap is normal to the crystallographic X-axis. Two arc-like parts around the half-moon electrodes are the electrode contact track used to connect the gold electrodes to an applied lateral electric field excitation source.

A crystal holder was used to install the LFE device during experiment. The two electrodes of the device are connected to external electric field source applied through the two contract springs inside the crystal holder. The device was measured using a network analyser HP8752A and the data were transported to PC through GPIB interface, as shown in Fig.7. During experiment, a 300 kHz frequency span was set for the convenience of analysing the performance nearly at resonance point. The experimental results were depicted using the reflection coefficient and admittance characteristic curve.

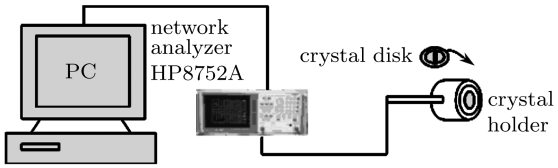


Fig.7. Experimental measurement system.

4. Results and discussion

The magnitude of reflection coefficient and the phase curve measured in air are shown in Fig.8, where there is a significant major resonance peak observed. It can be seen that the resonance frequency excited by lateral electric field is 4275938 Hz approximately in agreement with the above calculated result. It is believed that the mass effect of the electrodes results in a little lower resonant frequency.

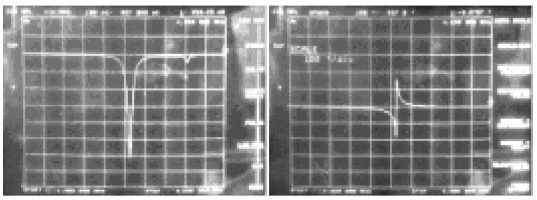


Fig.8. Reflection coefficient magnitude (left) and phase (right).

According to the operation theory of network analyser, the measured load impedance or admittance can be derived from its reflection coefficient and the normalized value of the network analyser which is often its characteristic impedance (50 Ω for HP8752A). Thus, the admittance as a function of frequency is calculated and its magnitude and phase curve are plotted with a grey solid line in Figs.9 and 10 respectively. It can be seen that the admittance characteristic curve is exactly similar to that of the unloaded TSM resonator in the TFE mode.[15] The figures show the resonance (f_r = 4275938 Hz) and anti-resonance (f_a = 4283550 Hz), where the admittance phase angle is zero and device reactance is zero. The admittance magnitude reaches its maximum value of 58.6 mS (corresponding to the impedance value of 17 Ω) at f_r. In Fig.10 there are other two zero-phase points observed but at f_r and f_a. It is believed that the other two resonances at a little higher frequency relative to f_a are probably introduced by additional LFE effect caused by the two opposite ends of a pair of electrode contact tracks.

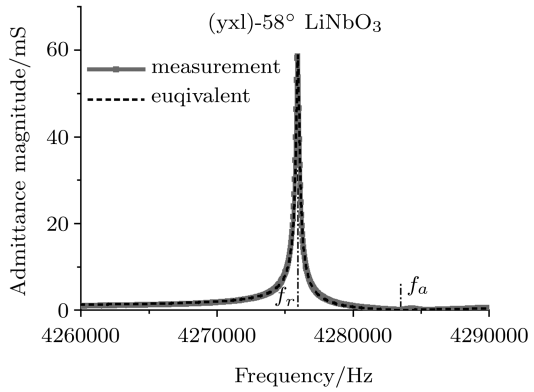


Fig.9. Admittance magnitude vs. frequency for (yxl)-58° $LiNbO_3$.

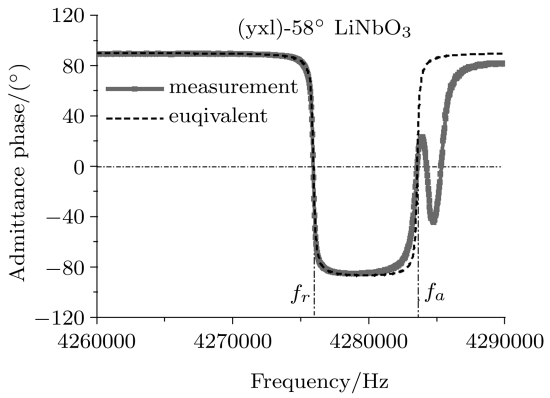


Fig.10. Admittance phase vs. frequency for (yxl)-58° $LiNbO_3$.

According to the half-power-point technique,[16] the Q-factor value at resonance (f_r) can be approximately calculated

$$Q = \frac{f_r}{|f_{+1/2} - f_{-1/2}|}, \tag{18}$$

where $f_{+1/2}$ and $f_{-1/2}$ are the frequencies which are higher and less than f_r at half power points on the resonant curve, respectively. From Fig.9, $f_{+1/2}$ and $f_{-1/2}$ are about 4276125 Hz and 4275712 Hz respectively and then the Q-factor value is calculated to be 10353 by using Eq.(18).

The measured admittance curve can be equivalent with the characteristic curve of a common BVD (Butterworth–Van Dyke) circuit, which is well known for its being used to describe a TSM resonator's behaviour. The BVD equivalent circuit is shown in Fig.11. When R_m = 17 Ω, L_m = 12 mH, C_m = 118 fF and C_0 = 33 pF, its admittance magnitude and phase

as a function of frequency is calculated and plotted with a thin shot-dashed line in Figs.9 and 10, respectively. It is clear that the equivalent curves are almost identical to the measured ones apart from a weak resonance occurring at a little higher frequency relative to f_a, which is probably caused by a pair of electrode contact tracks. This indicates that the TSM bulk acoustic wave excited by LFE has properties similar to that excited by TFE.

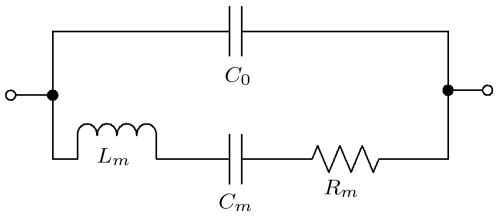


Fig.11. The BVD equivalent circuit of the (yxl)-58° $LiNbO_3$ LFE device.

For an LFE device, its motional resistance R_m caused by LFE at resonance is given by Eq.(19) in theory,[8]

$$R_m = \frac{(\pi/2)^2\alpha}{K^2\omega_r C_0}, \tag{19}$$

where α is the attenuation factor of the crystal material, K is the piezoelectric coupling factor, ω_r is the angular frequency at resonance, C_0 is the static capacitance of LFE devices determined in part by the electrode width W, gap width t and crystal substrate thickness d shown in Fig.12 and is given by

$$C_0 = \frac{\varepsilon_r\varepsilon_0 W d}{t}, \tag{20}$$

where ε_r is the relative permittivity of crystal substrate and ε_0 is the permittivity of vacuum. The attenuation factor α is determined by

$$\alpha = \frac{\eta\omega_r^2}{2V_a^3\rho}, \tag{21}$$

where η is the viscosity of crystal material, V_a is the acoustic wave phase velocity and ρ is density of crystal material. Substituting Eqs.(21) and (20) into Eq.(19) and using Eq.(17) when $N = 1$, we obtain the approximate motional resistance R_m of an LFE device,

$$R_m = \frac{\pi^2\eta t}{8K^2\rho V_a^2\varepsilon_r\varepsilon_0 A}. \tag{22}$$

In order to compare with the (yxl)-58° $LiNbO_3$ LFE device, a 5 MHz AT-cut LFE device (quartz) was also fabricated by the same method as the above and shown in Fig.6 (right). Here the electrode gap of AT-cut LFE device is made parallel to the X-axis in order to excite a pure c mode TSM due to its maximum LFE

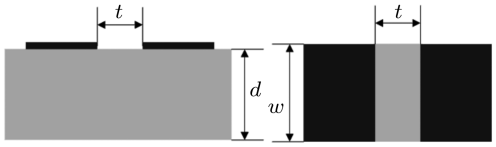


Fig.12. Geometry size of typical LFE device configuration. The black stands for electrode and the grey for substrate.

coupling when $\psi = 90°$, as different from the (yxl)-58° $LiNbO_3$. Its parameters concerned were calculated and shown in Table 2 together with those of $LiNbO_3$. As their acoustic wave phase velocity V_a, mass density ρ, viscosity coefficient η and area A are nearly in the same order, the difference between the two motional resistances is mainly caused by the piezoelectric coupling factor K and the relative permittivity ε_{11}. By using Eq.(22) and Table 2, the R_m of the AT-cut quartz can be calculated, which is beyond 6000 times higher than that of (yxl)-58° $LiNbO_3$, as is also verified by similar test done on AT-cut LFE quartz device. And the result shows that there is not any major resonance peak observed in air due to its very high motional resistance. This indicates that if very high coupling and high dielectric materials (e.g., $LiNbO_3$) are used, the motional resistance of the LFE device at resonance will be much lower.

Table 2. Comparison between LFE quartz and $LiNbO_3$.

LFE device	V_a/(m/s)	K	ρ/(kg/m^3)	ε_{11}
Quartz	3315	6%	2650	4.5
$LiNbO_3$	3983	95.46%	4640	44

5. Conclusions

Bulk acoustic wave propagation properties of $LiNbO_3$ single crystal excited by lateral electric field have been investigated. It is found that the maximum LFE coupling factor for c mode in all different cut orientations and lateral field directions is much higher than for the other two (a and b) modes. For both the (yxl)-58° and (yxwl)±60°/58° substrates, the LFE coupling factor for c mode reaches its maximum value of 95.46% when $\psi = 0°$, whereas it is zero for a and b modes. This indicates that a pure LFE shear mode (c

mode) with very high coupling factor exists for $\psi = 0°$. The phase velocity of c mode shear wave changes from 3456 to 3983 m/s as a function of ψ. A 5 MHz LFE device of (yxl)-58° $LiNbO_3$ with $\psi = 0°$ was designed and tested in air. A major resonance peak with the motional resistance as low as 17 Ω and the Q-factor value up to 10353 was observed. The resonance caused by LFE for (yxl)-58° $LiNbO_3$ device occurs more easily in air compared to the common crystal materials, e.g., quartz, due to its high coupling and high dielectric performance. The test result is in good agreement with the theoretical analysis, and suggests that the LFE $LiNbO_3$ device can be a good platform for high performance resonator or sensor applications.

References

[1] Mecea V 1994 *Sens. Actuators* A **40** 1

[2] Martin S J, Frye G C and Wessendorf K O 1994 *Sens. Actuators* A **44** 209

[3] Martin S J, Granstaff V E and Frye G C 1991 *Anal. Chem.* **63** 2272

[4] Ballato A, Hatch E R, Mizan M and Lukaszek T J 1986 *IEEE Trans. Ultrason., Ferroelect., Freq. Contr.* **33** 385

[5] Atanasoff J V and Hart P J 1941 *Phys. Rev.* **59** 85

[6] Hruska C K and Kucera M 1985 *IEEE Trans. Ultrason., Ferroelect., Freq. Contr.* **SU-32** 600

[7] Auld B A 1973 *Acoustic Fields and Waves in Solids* (Volume I) (New York: Wiley) p357

[8] Rosenbaum J F 1988 *Bulk Acoustic Wave Theory and Devices* (Boston, MA: Artech House)

[9] Turner E H 1966 *Appl. Phys. Lett.* **8** 303

[10] Changho L, Yongbae J and Kwangsoo N 2003 *Opt. Engin.* **42** 1589

[11] Collins J H, Gerard H M and Shaw H J 1968 *Appl. Phys. Lett.* **13** 312

[12] Lee T C, Lee J T, Robert M A, Wang S and Rabson T A 2003 *Appl. Phys. Lett.* **82** 191

[13] Ballato A, Hatch E, Lukaszek T and Mizan M 1986 *Proc. IEEE 1986 Ultrason. Symp.* 339

[14] Khan A and Ballato A 2002 *IEEE Trans. Ultrason., Ferroelect., Freq. Contr.* **49** 922

[15] Ballantine D S, White R M, Martin S J, Zellers E T and Wohltjen H 1997 *Acoustic Wave Sensors: Theory, Desigh, and Physico-Chemical Applications* (San Diego: Academic) p53

[16] Luo Y L 1996 *Microwave and Opt. Technol. Lett.* **11** 18